Received: 1 November 2019 | Revised: 27 November 2019 | Accepted: 1 December 2019

DOI: 10.1002/inf2.12075

ORIGINAL ARTICLE

WILEY

A biomimetic-structured wood-derived carbon sponge with highly compressible and biocompatible properties for human-motion detection

Yipeng Chen[1] | **Lintong Hu**[2] | **Caicai Li**[1] | **Baokang Dang**[1] | **Qingfeng Sun**[1] | **Tianyou Zhai**[2] | **Huiqiao Li**[2]

[1]School of Engineering, Zhejiang A&F University, Hangzhou, China

[2]State Key Laboratory of Material Processing and Die & Mould Technology, School of Materials Science and Engineering, Huazhong University of Science and Technology, Wuhan, China

Correspondence
Qingfeng Sun and Huiqiao Li, School of Engineering, Zhejiang A&F University, Hangzhou 311300, China.
Email: qfsun@zafu.edu.cn (Q. S.); hqli@hust.edu.cn (H. L.)

Funding information
Hubei Provincial Natural Science Foundation of China, Grant/Award Number: 2019CFA002; National Basic Research Program of China, Grant/Award Number: 2015CB932600; the Fundamental Research Funds for the Central University, Grant/Award Number: 2019kfyXMBZ018; Zhejiang Provincial Natural Science Foundation for Distinguished Young Scholars of China, Grant/Award Number: LR19C160001

Abstract

Piezoresistive sensors, as an indispensable part of electronic and intelligent wearable devices, are often hindered by nonrenewable resources (graphene, conventional metal, or silicon). Biomass-derived carbonaceous materials boast many advantages such as their light weight, renewability, and excellent chemical stabilization. However, a major challenge is that the strength and resilience of carbon-based piezoresistive materials still falls short of requirements due to their random microarchitectures which cannot provide sufficiently good stress distribution. Encouraged by the excellent compressible properties and extraordinary strength of the *Thalia dealbata* stem, we propose a wood biomass-derived carbon piezoresistive sensor with an artificial interconnected lamellar structure like the stem itself. By introducing a freezing-induced assembly process, a wood-based, completely delignified, nano-lignocellulose material can be built into a "bridges supported lamellar" type architecture, where subsequent freeze-drying and pyrolysis results in carbon aerogel monoliths. The resultant bioinspired carbon sponge has high compressibility and strength, of the order of two to five times higher than that of conventional metal, carbon, and organic materials. Combined with excellent biocompatible properties and chemical durability, these are useful properties for intelligent wearable devices and human-motion detection.

KEYWORDS

biocompatible property, biomimetic, carbon material, compressible property, lignocellulose, piezoresistive sensors

1 | INTRODUCTION

Piezoresistive sensors are used in many industrial applications, especially in wearable electronics and intelligent systems, to convert applied compressive stress or strain into resistance signals.[1-5] They can be installed on the human body or on clothing to constantly monitor subtle or large body motion[6-8] and physical information.[9-12] Since these applications require lightweight, weather-resistant sensors, capable of skin contact, the

This is an open access article under the terms of the Creative Commons Attribution License, which permits use, distribution and reproduction in any medium, provided the original work is properly cited.
© 2020 The Authors. *InfoMat* published by John Wiley & Sons Australia, Ltd on behalf of UESTC.

designed sensors should possess a number of basic characteristics, such as superior sensitivity, excellent flexibility, light weight, biocompatibility, and suitable stability. Consequently, lightweight and compressible carbonaceous materials are increasingly being used as alternative piezoresistive materials in the industry. However, these carbon units are usually prepared from nonrenewable resources such as fullerenes, graphene, carbon nanotubes, resorcinol formaldehyde granules, and so on, which are generally complicated by toxic reagents, complex equipment, high process requirements, and low productivity.[13,14] Biomass-derived carbons are renewable and abundant, which provides an attractive and simple alternative to the construction of compressible carbon sensors.[15,16] However, the resulting materials exhibit unsatisfying strength and resilience due to the difficulty of property manipulation and the lack of suitable mechanical structure. To enhance their performance, rational design of a suitably robust microstructure is of great importance for such biomass-derived material.

Examples from nature provide abundant inspiration for the design and development of such materials.[17-19] Numerous natural materials (eg, plant stems) are elongated and robust owing to their complex layered structures, from nano/micro to macro levels.[20] Although porous and weak in composition, they have excellent mechanical properties.[21] The stem of *Thalia dealbata*, for example, has a layered structure connected by interlayer bridges that make it robust, elastic, and light enough to survive in recurrent high winds.[22]

Herein, we develop a new type of lightweight and flexible piezoresistive sensor by reconstructing the abundant and sustainable wood-derived nanofibrillated cellulose (NFC) into a carbon sponge. Inspired by the "bridges supported lamellar" architecture of the *T. dealbata* stem, a freezing-induced strategy was designed[23] to create the bioinspired architecture carbonaceous nanofibrous sponge (BCS) from wood-derived NFC. This BCS not only imitates the structural characteristics of the plant stem, but also has excellent strength and elasticity, some 1.5 to 5 times higher than that of conventional metal, carbon, and organic materials. This promises appealing opportunities as a reused and regenerated material for piezoresistive sensors. This approach also provides a universal way of enhancing the mechanical properties of biomass-based materials, chiefly in strength and resilience. Experiments confirmed that BCS shows higher biocompatibility than conventional silicone-based sensors toward human umbilical vein endothelial cells (HUVECs), and has better corrosion resistance and chemical stability than traditional metal sensors. Combined with outstanding mechanical and chemical durability, these biocompatible properties make BCS a promising candidate in wearable electronics and intelligent system applications.

2 | RESULTS AND DISCUSSION

Figure 1A-C shows the configuration of the *T. dealbata* stem. The digital photograph in Figure 1A shows the macroscopic morphology of *T. dealbata*. Its stem can be more than 2 m tall, yet just 5 to 10 mm thick, and still be robust and elastic enough to survive in the high winds of its country of origin (the southern United States and tropical areas of Mexico). A "directional layered structure with interconnected bridges" is observed in the SEM images (Figure 1B,C) of the stem. The thickness of the sheet is 15 to 20 μm and the length of the bridge is 5 to 10 μm.

The synthesis process of BCS is shown in Figure 1D. The wood-NFC was prepared and isolated by the removal of lignin/hemicellulose from the lignocellulose during the mechanochemical process using a colloid grinder (Figure S1). Transmission electron microscopy (TEM) of the wood-NFC showed that the lignocellulose was completely transformed into nanofibers several microns long and 10 to 50 nm wide (-Figure S2). Subsequently a homogeneous nanofiber dispersion was formed by agitating the wood-NFC dispersion with konjac glucomannan (KGM; 100 wt% relative to wood-NFC), followed by further stirring. The freezing-induced assembly technique (Figure S3) was used to duplicate a hierarchical architecture in wood-derived NFC/KGM, upon freezing the partially reduced wood-derived NFC/KGM was excluded from the formed ice and sandwiched between adjacent ice crystals to take the shape of a continuous network, whose structure was determined by the shape of ice crystals.[21] The wood-NFC/KGM aerogel was manufactured by means of freeze-drying of the dispersion (Figure S4). The prepared wood-NFC/KGM aerogel was completely stripped down at 90°C (Figure S5) and then carbonized at 900°C to prepare the BCS. Figure 1E shows that a typical BCS (85 mg cm^{-1}), which is itself easily supported by leaves, can bear weight of up to 5000 times itself with about 70% strain (Figure 1F), demonstrating the high specific strength of BCS (Figure S6).

SEM analysis showed that the lamellar structure was conserved well after elevated temperature (900°C) carbonization. Figure 2A,B show the random carbon aerogel obtained from carbonizing the random wood fiber aerogel with messy mesh, including carbon fiber of 5 to 20 mm in diameter. The BCS proves to be a totally different structure to that of the random carbon aerogel

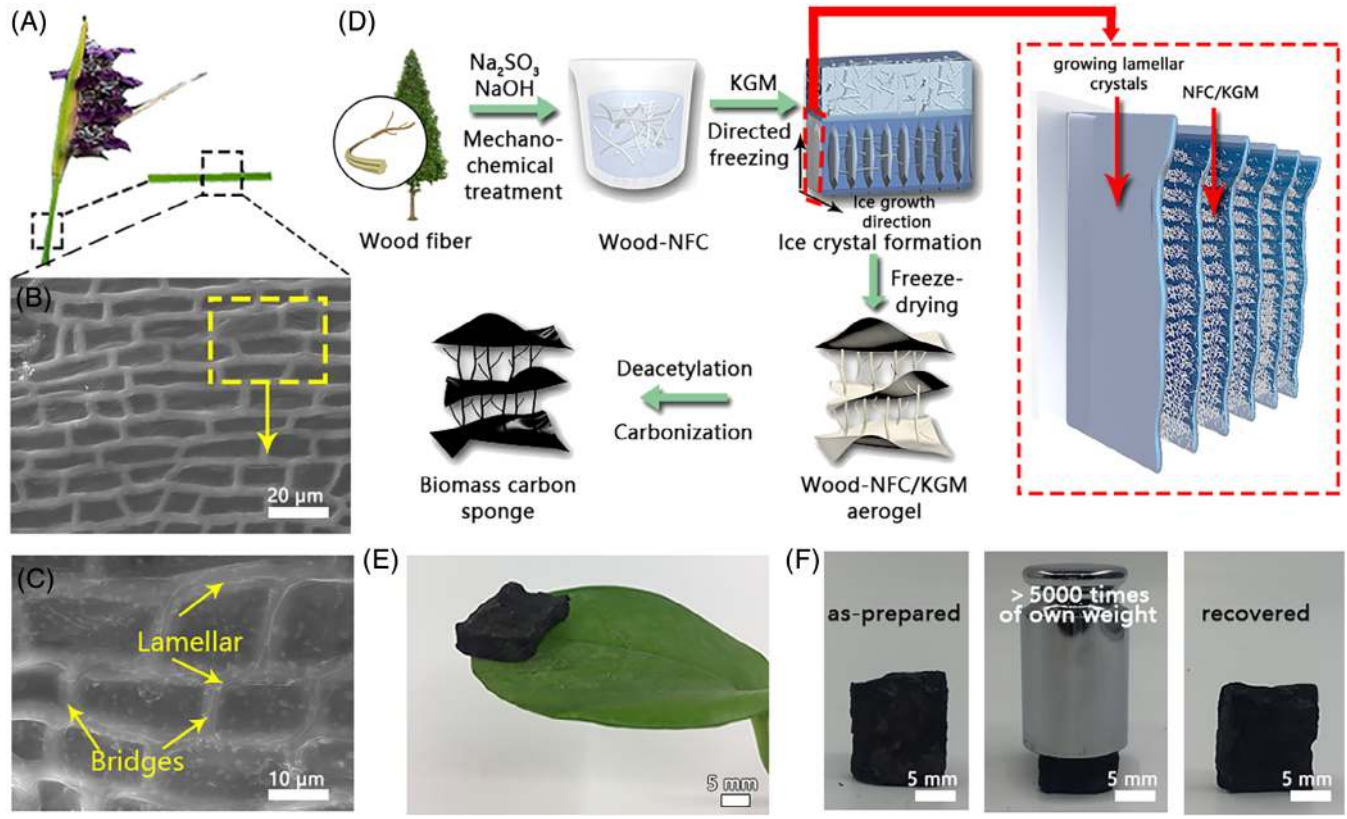


FIGURE 1 A, Digital photo and (B and C) SEM images of a *Thalia dealbata* stem. D, Schematic representation of the design and manufacturing process of a BCS. E, An optical photograph showing a BCS on the tip of a leaf. F, Optical images showing a BCS which bears the weight that up on 5000 times its own weight with about 70% strain. BCS, bioinspired architecture carbonaceous nanofibrous sponge

structure. Nevertheless the "bridges (length: 10-20 μm) supported lamellas" (thickness: approximately 12 μm) structure of the *T. dealbata* stem was mimicked and obtained (Figure 2F,G). Figure 2C-E,H-J validate the mechanical compressibility of the two different carbon materials. Due to their high porosity, both types of carbon bulk can be compressed by more than 75%. However, the random carbon aerogel bulk is permanently deformed after being compressed by more than 75% (Figure 2C-E). The BCS bulk, however, completely reverts to its original shape under the same degree of compression (Figure 2H-J), demonstrating its excellent mechanical compressibility.

Figure 3A exhibits three obvious regions of the stress–strain (σ-ε) curves: a linear-elastic region for $\varepsilon < 25\%$ records the elastic bending of the BCS, a plateau region for $25\% < \varepsilon < 50\%$ corresponding to the elastic buckling of the BCS, and a densification region for $\varepsilon > 50\%$ with σ increasing rapidly. The maximum stress is 61.6 kPa at 75% strain. Energy dissipation[24] measurements were performed to further characterize energy absorption competency of our bioinspired BCS. Figure 3B shows the energy loss coefficient of the BCS reduces from 61% to 29% over the 1000 cycle compression test and the BCS retained >70% of the original maximum stress. As shown in Figure 3C, dynamic viscoelastic measurements showed that the storage (E') and loss (E'') modulus of the BCS were almost stable and independent over the entire range of angular frequency (ν) (1-100 Hz) tested. To further investigate the exceptional mechanical properties of the BCS, we compared our bioinspired BCS with carbon aerogel with random structure (Figure 3D-F). The bioinspired BCS and the random carbon aerogel were prepared by directionally and conventional unidirectionally freezing a suspension of wood-NFC/KGM (1:1) at −90°C, respectively. Despite similar densities (80-89 mg cm^{-3}), the two types of carbon materials exhibited different compressive behaviors (Figure 3D,E). For the bioinspired BCS, after 50% compression, the maximum compression stress was 15.3 (Figure 3D), and the maximum stress remained 87% after 1000 cycles (Figure 3F). Although the density of the bioinspired BCS is similar to that of random carbon aerogels and there is no noticeable difference in maximum stress, the robustness, and elasticity of the random carbon aerogel was far worse, retaining just 35% of its maximum stress after only 20 compressive cycles at 50% compressive strain (Figures 3F and S5). To correlate the mechanical

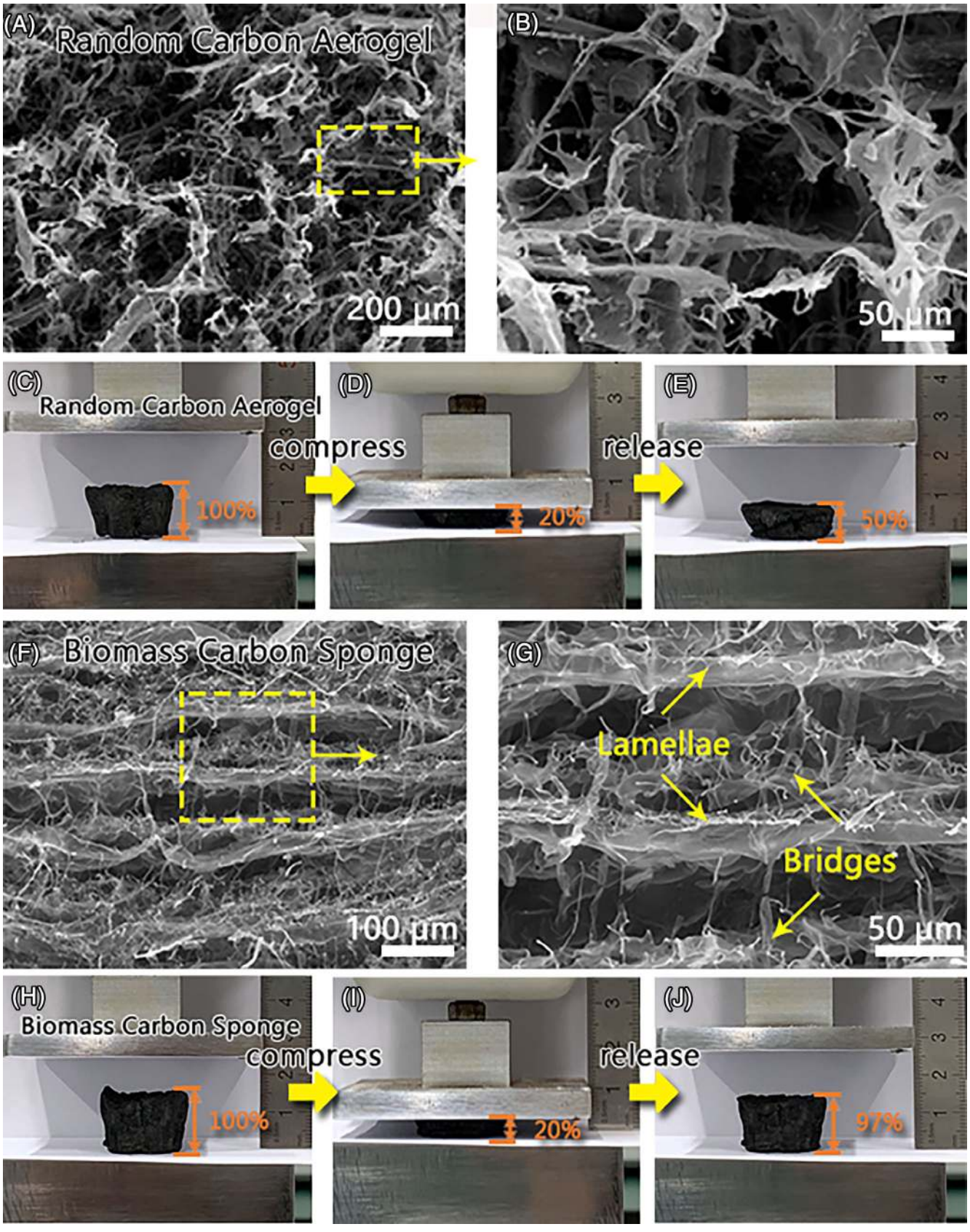


FIGURE 2 Legend on next page.

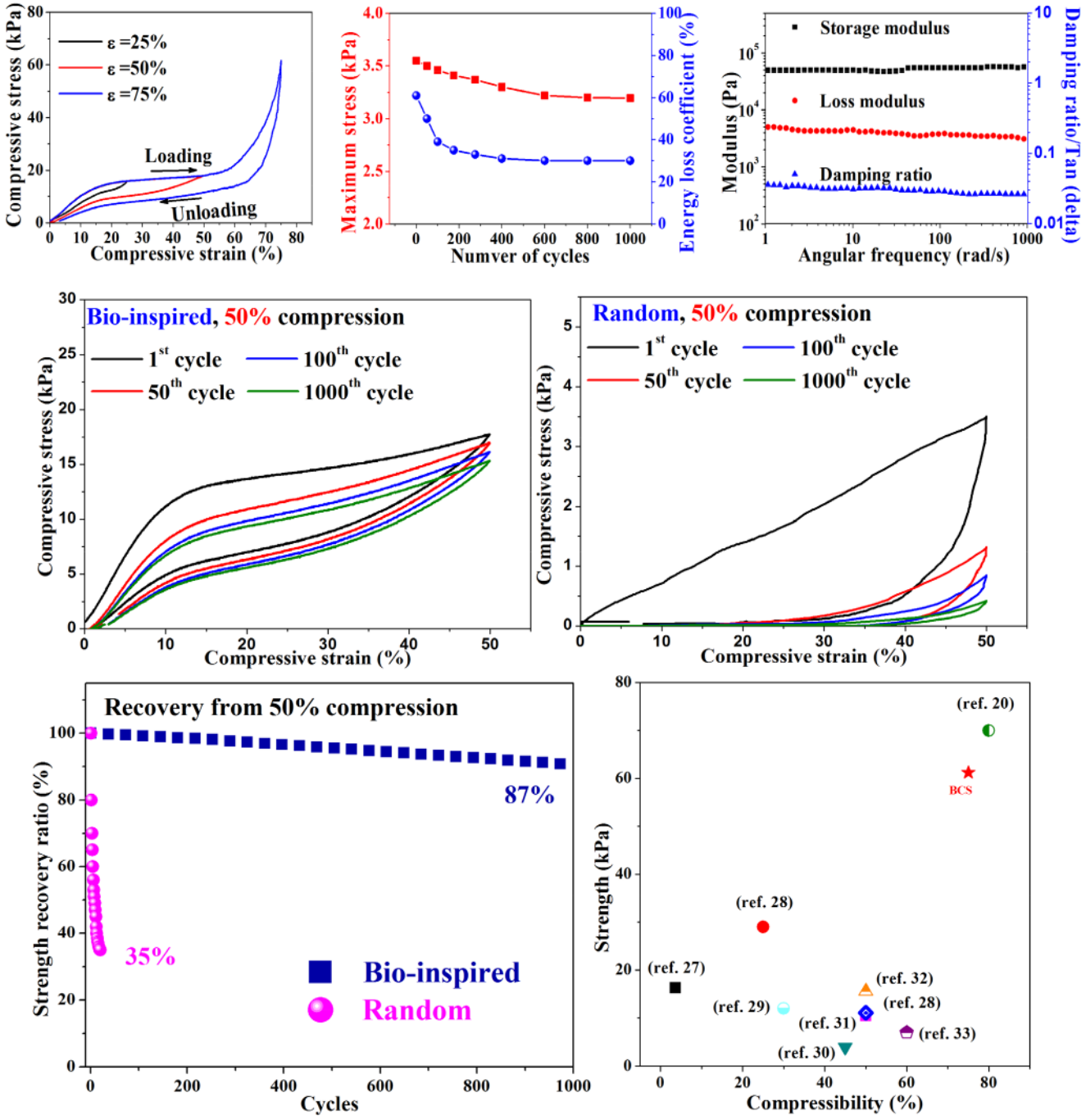


FIGURE 3 A, Compressive σ vs ε curves for BCS at different set ε. B, Energy loss coefficient and maximum stress of the bioinspired BCS during 1000 cycles. C, The frequency dependence of storage modulus, loss modulus, and the damping ratio of BCS. D and E, 1000 cyclic fatigue compressive test with the bioinspired BCS and random aerogels. F, Final strength of the bioinspired and random aerogel after 1000 and 20 cycles, respectively. G, Plot of compressibility and strength of BCS compared with that of general metal, carbon, and polymer-based materials. BCS, bioinspired architecture carbonaceous nanofibrous sponge

FIGURE 2 A and B, Microscopic structure of random carbon aerogel at different magnifications. C–E, Photographs of the random carbon aerogel bulk before compression, C, under compression, D, and after release, E. G, Microscopic structure of BCS at different magnifications. H–J, Photographs of the random carbon aerogel bulk before compression, H, under compression, I, and after release, J. BCS, bioinspired architecture carbonaceous nanofibrous sponge

behavior of the carbon material with their microstructures, the microscale structures of bioinspired BCS and random carbon aerogel were traced, both before and after compressive cycles at 50% compressive strain. Although there are some previously reported carbon and polymer-based materials with high compressibility, their strengths are ordinary, and while some metallic microlattices show high strength, their compressibility is poor.[16,25-31] The BCS show extraordinary strength and resilience, some 1.5 to 5 times higher than that of general metal, carbon, and polymer-based materials (Figure 3G).

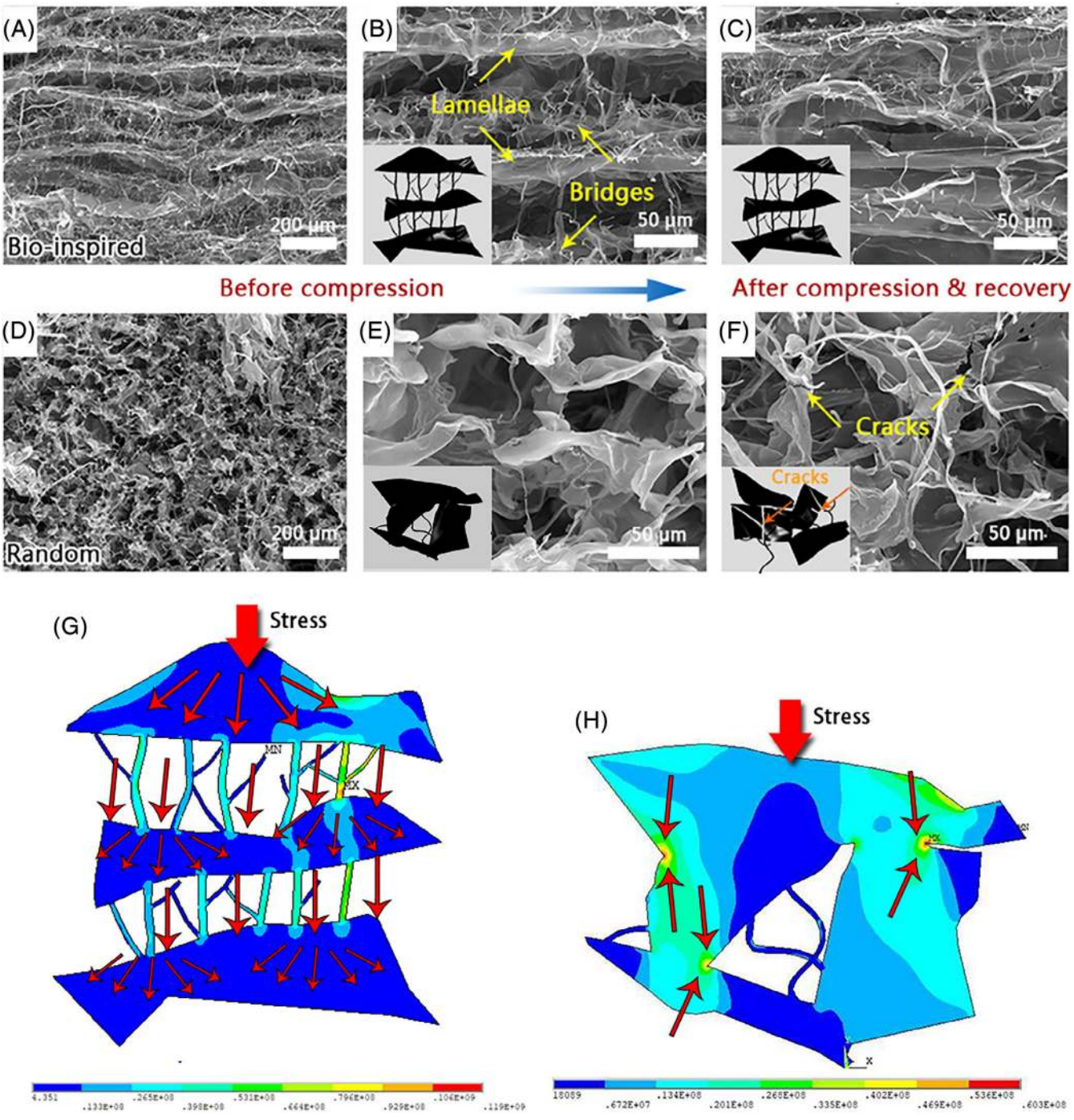


FIGURE 4 A and B, SEM images of BCS before compression. C, Magnified SEM images of BCS after 100 cycles of compression. D and E, SEM images of random carbon aerogels before compression. F, Magnified random carbon aerogels of BCS after 100 cycles of compression. The schematics of stress spread over the, G, BCS and, H, random aerogels under large geometry deformation. BCS, bioinspired architecture carbonaceous nanofibrous sponge

As shown in Figure 4A-C, the bioinspired BCS shows a long-range layered structure and bridge. For better illustration, the insets also show a schematic drawing of its architectural features. In the process of compression, the stress can be diffused to the whole plate, avoiding stress concentration.[16,32] The interconnected bridges play a role of many "springs" between each layer, and elastic deformation is dominant in the compression cycle (Figure 4G). The BCS was completely restored to its original state after compression, and damage was not obvious (Figure 4C). As shown in Figure 4D–F, the random carbon aerogel exhibits haphazardly lamellar layers, which have similar thickness to that of the bioinspired BCS. The schematics show that the stress area is more local and

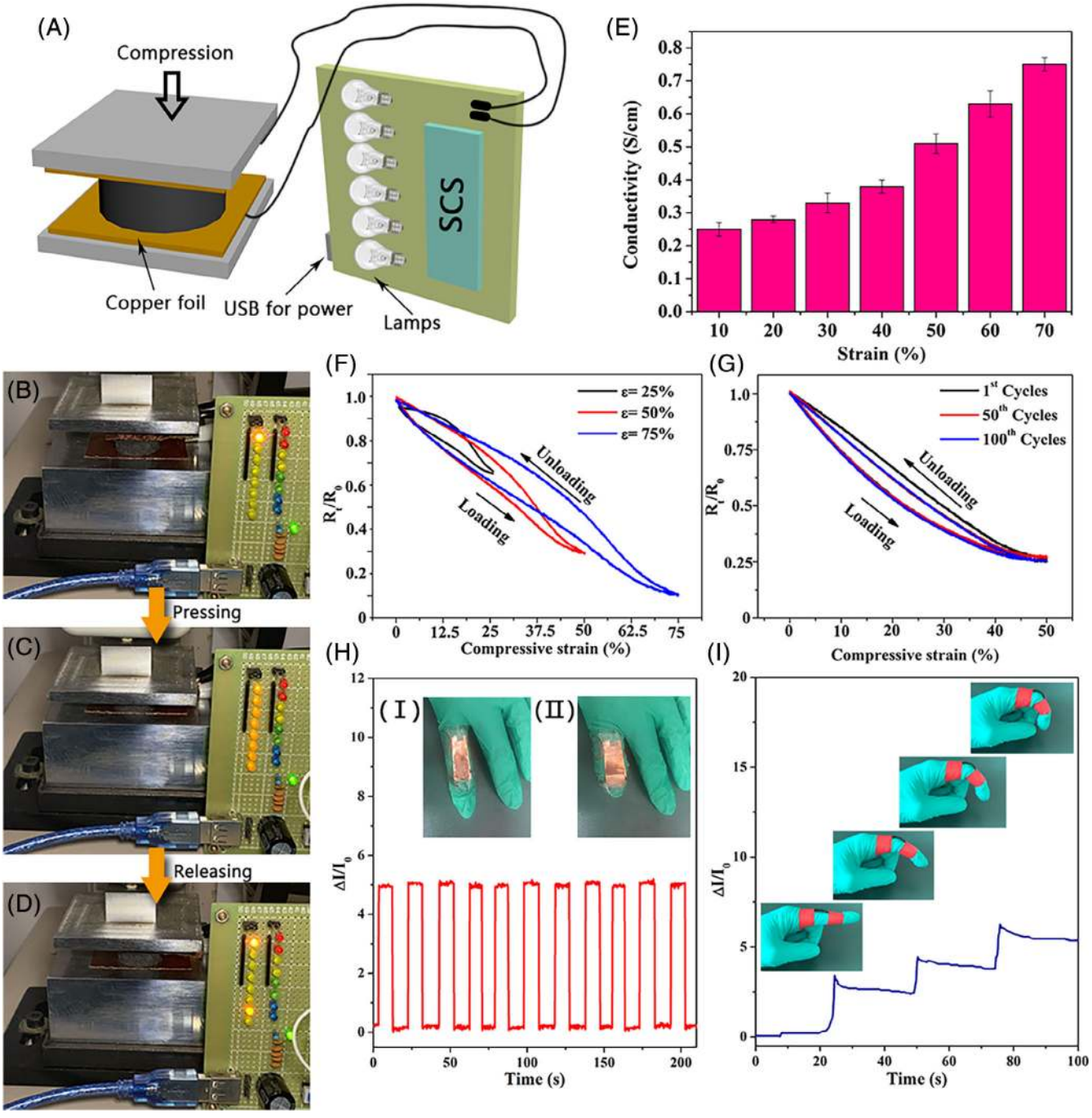


FIGURE 5 A-D, Pressure-sensitive behavior of a representative BCS. E, Electrical conductivity of BCS as a function of compressive strain. F, Resistance variation vs compressive strain for BCS. G, 100-cycle piezoresistive resistance test with compressive strain of 50%. H and I, Current changes ($\Delta I/I_0$) under different progressive motions of the piezoresistive sensor on a finger, shown as insets. BCS, bioinspired architecture carbonaceous nanofibrous sponge

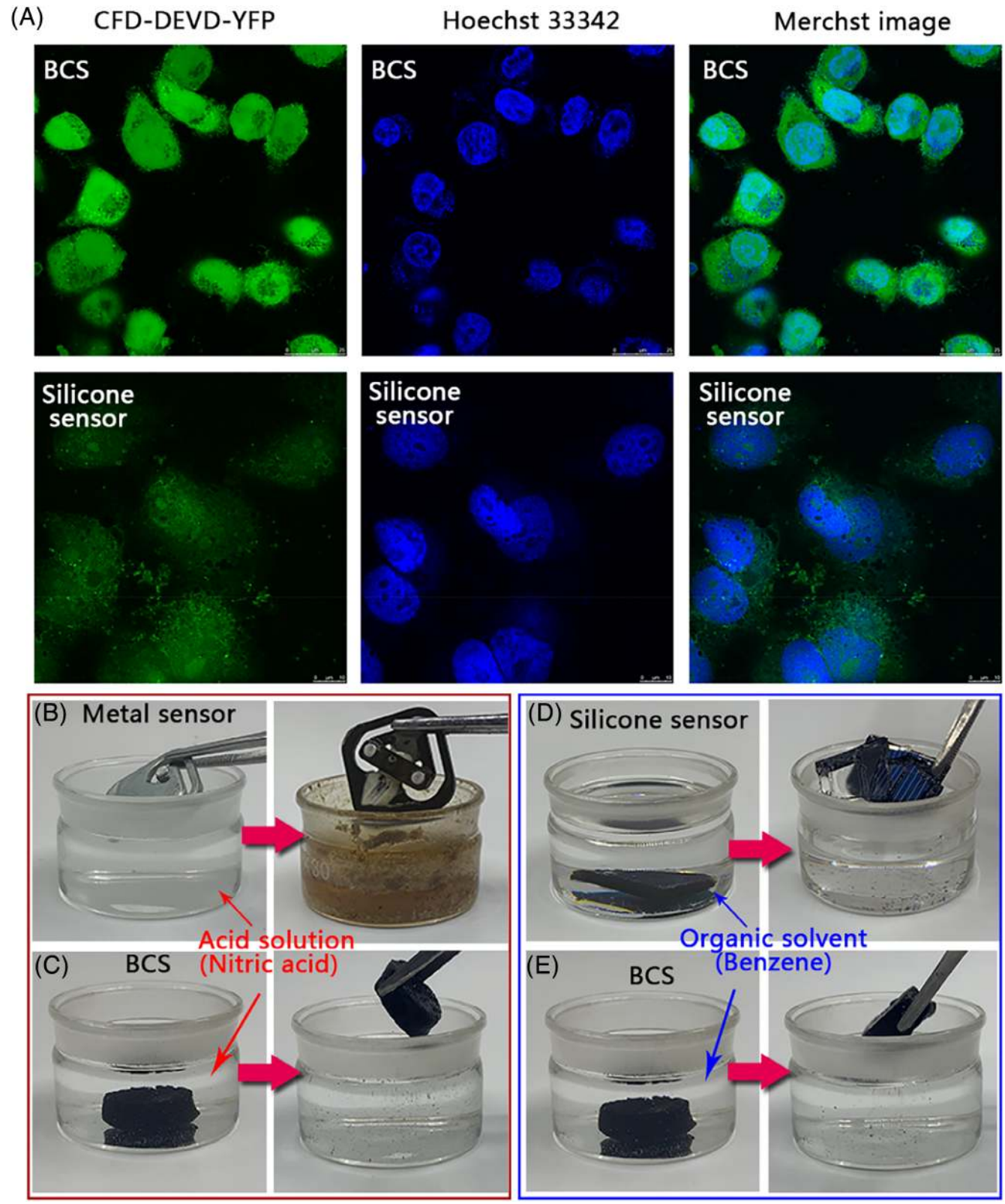


FIGURE 6 A, Fluorescence images of HUVECs on the BCS and silicone sensor for 48 hours. The green fluorescence and the blue fluorescence are attributed to the CFP-DEVD-YFP4 fusion protein, and Hoechst 33342, respectively. B, The chemical stability of the metal sensor, B, and silicone sensor, D, in nitric acid and benzene is compared with that of BCS, C and E, respectively. BCS, bioinspired architecture carbonaceous nanofibrous sponge; HUVEC, human umbilical vein endothelial cell

concentrated than the bioinspired BCS (inset of Figure 4D—F,H). The final performance depends on the vulnerable areas in the random structure. In the process of compression, the weakest part is prone to crack, leading to inelastic deformation and a lack of elasticity. The SEM images and compressive tests show that the BCS with "bridges supported lamellars" structure is more resilient than the random carbon aerogel structure.

Transmission electron microscopy observation of the BCS revealed that carbonizing NFCs were embedded in ultrathin carbon sheets and maintained the fibrous configuration during pyrolysis (Figure S7). In addition, 1D of constructional carbon sheets were observed, which contributed to improving their mechanical performance.[33,34] X-ray diffraction (XRD) and Raman spectroscopy also provide evidence for the composition of carbon structures (Figures S8 and S9). Furthermore, the wood-NFC/KGM aerogel usually produces significant volume shrinkage during pyrolysis, while carbonizing wood-NFC supports the aerogel and prevents its collapse (Figures S6A and S10). The electrical conductivities of BCS-800 and BCS-900 are 0.23 and 0.32 S/cm. The components of the BCS were verified by X-ray photoelectron spectra (XPS), and were C (>85.3 wt%), and O (<7.3 wt%, Figures S11B and S9, Table S1). Unsurprisingly, there was an obviously increase in the C contents of the BCS with the pyrolysis temperatures.

A piezoresistive sensor devised through a single chip system was connected with the BCS in a circuit (Figure 5B-D). The equipment diagram is shown in Figure 5A. The number of light bulbs lit gradually increases and decreases during a pressing-releasing cycle at 50% compressive strain, indicating the piezoresistive conductivity of the BCS. The conductivity of the BCS increases with the progressive strain, which was increased from 0.25 to 0.38 S/cm by the addition of 30% compressive strain. As the strain further increased, it gradually increased to about 0.75 S/cm. Figure 5F shows the resistance variation (R_t/R_0) vs compressive strain for the loading-unloading cycle at maximum strains of 25%, 50%, and 75%, demonstrating that R_t/R_0 reduced with increased compressive strain and recovered its initial value after the strain was released. Furthermore, to show the stability and reversibility of BCS, its fatigue testing was recorded for 100 cycles (Figure 5G), which is shown as a function of cyclic vs strain (Figure S12). In recent years, flexible strain sensors with high piezoresistive sensitivity can be used in human activities and health monitors, and other related applications.[1,24] To confirm the application prospect of the BCS as a piezoresistive sensor, the BCS sensor was installed on a human finger (inset in Figure 5H and Figure S13). When the finger moved from straight (I) to curved (II), the relative current of the sensor increased (Figure 5H), indicating a recurrent square wave signal after several cycles. The current changes were observed, when the finger bent to a certain angle, as shown in (Figure 5I). These results support the use of the BCS as a piezoresistive sensor for various applications.

Regarding applications in human monitors, sensors installed on human body or clothing need to have excellent biocompatibility. HUVECs was cultured on the BCS to evaluate their cytotoxicity. Because the CFP-DEVD-YFP fusion gene encodes the C3 sensor protein, the HUVECs can consistently emit green fluorescence.[35,36] Hoechst 33342 is a fluorescent dye that marks DNA specifically and is used to restain the nuclei of living HUVECs. Figure 6A shows that HUVECs dispersing on the BCS are flat with a central nucleus, and HUVECs exhibit a higher uptake of the BCS than that of the silicon sensor, indicating that the BCS is more appropriate for supporting cell growth than the silicon sensor. The intense green fluorescence further confirmed that HUVECs were alive and had normal metabolism. The viability of HUVECs on the BCS was examined by an MTT (3-(4, 5-dimethyl-2-thiazolyl)-2, 5-diphenyl-2*H*-tetrazolium bromide) experiment. As shown in Figure S14, the relative cell viability increased with culture time. The relative viability of HUVECs on the BCS was significantly more than that on the silicon sensor when the experiment was completed (Figure S14). Thus, the BCS was considered cytotoxicity free for HUVECs. Due to the use of piezoresistive sensors needing to cope with different external environments including a variety of reagents, the chemical durability of the BCS was evaluated. The BCS was placed into a nitric acid solution with a pH of one and benzene (Figure 6C,E), retaining its original electric-stress response performance after being removed from these solutions (Figure S15). Conversely, the metal sensor (Figure 6B) and the silicon sensor (Figure 6D) were corroded and dissolved in the nitric acid solution and benzene, respectively. Overall, the BCS in this study was biocompatible, and exhibited chemically stable substrates for cell adhesion and growth, which is a potential useful material with many applications, such as tissue engineering and health monitoring, especially in systems requiring high chemical durability and high strength.

3 | CONCLUSIONS

In summary, the BCS with the lamellar structure inspired by the *T. dealbata* plant stem was fabricated by using a freezing-induced assembly process based on an abundant, green biomass-based material. This bioinspired

construction of layered structures and interconnected bridges provides the BCS with extraordinary strength and elasticity. With good biocompatibility, and chemical stability, we envisage that the BCS will provide a new concept for a range of applications in wearable electronics, health monitoring and tissue engineering. The fabrication of sustainable natural materials into high value-added carbon materials opens up myriad opportunities for the development of renewable materials.

4 | EXPERIMENTAL SECTION

4.1 | Material

The raw materials, never-dried wood fiber (*Populus ussuriensis Kom*) were kindly provided by Henan Province Jiaozuo National Forestry Farm. Konjac gum was provided by Linankar Biotechnology Co., Ltd. NaOH and Na_2SO_3 was used as received from Shang Hai Aladdin Industrial Co., Ltd.

Synthesis of Wood-NFC by the mechanochemical method: Wood fiber was suspended in a 2.5 M NaOH and 0.4 M Na_2SO_3 solution. Then the suspension was added to a colloid grinder and mechanochemically prepared for 12 hours. At this stage, the lignin/hemicellulose content of lignocellulose in the mechanochemical process was completely removed, mainly attributable to the different stabilities of lignin, cellulose, and hemicellulose in the NaOH and Na_2SO_3 solution, undergoing splitting, breaking, and refinement to nanoscale by mechanical force, followed by immersion in boiling deionized water several times to remove the chemicals.

4.2 | Synthesis of wood-derived carbon aerogels

Three grams of wood-NFC was homogenized at a speed of 13 000 RPM for 20 minutes and dispersed in 200 mL pure water to obtain uniform dispersion. Then 3 g KGM and 0.03 g NaOH was added, and continually stirred for 20 minutes. Subsequently, the solution was precooled to 4°C and poured into the polydimethylsiloxane (PDMS; Dow Corning Sylgard 184) mold. During the well-controlled freezing process, the water crystallized directionally and chitosan as the solute was extruded to form parallel layers between the ice crystals (Figure S3). The frozen matrix was dried in vacuo in a Labconco FreeZone 6 freeze dryer, and then treated in an oven at 80°C for 4 hours. The completely dried wood-NFC/KGM matrix was then heated at 90°C for 1 hour for deacetylation. To obtain the BCS, the deacetylated wood-NFC/KGM matrix was calcined at 900°C under flowing argon gas for 40 minutes.

4.3 | Characterization

The SEM and TEM images were obtained by Hitachi S-4800 and Tecnai G2 F20, respectively. The chemical structure of the BCS was measured by XRD (Panalytical Empyrean instrument), Raman spectroscopy (Renishaw RM2000), XPS (Thermo Fisher Scientific-K-Alpha 1063). The density (apparent density) of the BCS was measured as weight (w) divided by volume (v). Compression tests were measured using an Instron 5943. The elasticity-dependent electrical conductivity was measured by attaching copper wire leads to the flat surfaces of the cylindrical BCS with silver paste (DuPont 4929N) and using a EC-Lab V10 and Fluke Ohmmeter to measure resistance of both types of BCS vs strain. Dynamic compressive viscoelastic measurements of the BCS were performed using a Bose Enduratec ELF3200 DMA instrument.

ACKNOWLEDGMENTS

This work was supported by the Zhejiang Provincial Natural Science Foundation for Distinguished Young Scholars of China (Grant No. LR19C160001), Hubei Provincial Natural Science Foundation of China (2019CFA002), and the Fundamental Research Funds for the Central University (2019kfyXMBZ018), and the Analytical and Testing Center of HUST for the measurements.

CONFLICT OF INTEREST

The authors declare no conflict of interest.

ORCID

Tianyou Zhai https://orcid.org/0000-0003-0985-4806
Huiqiao Li https://orcid.org/0000-0001-8114-2542

REFERENCES

1. Yamada T, Hayamizu Y, Yamamoto Y, et al. A stretchable carbon nanotube strain sensor for human-motion detection. *Nat Nanotechnol*. 2011;6:296-301.
2. Amjadi M, Kyung KU, Park I, Sitti M. Stretchable, skin-mountable, and wearable strain sensors and their potential applications: a review. *Adv Funct Mater*. 2016;26:1678-1698.
3. Chen K, Gao W, Emaminejad S, et al. Printed carbon nanotube electronics and sensor systems. *Adv Mater*. 2016;28:4397-4414.
4. Rim YS, Bae SH, Chen H, De Marco N, Yang Y. Recent progress in materials and devices toward printable and flexible sensors. *Adv Mater*. 2016;28:4415-4440.
5. Trung TQ, Lee NE. Flexible and stretchable physical sensor integrated platforms for wearable human-activity monitoring and personal healthcare. *Adv Mater*. 2016;28:4338-4372.

6. Wang Y, Wang L, Yang T, et al. Wearable and highly sensitive graphene strain sensors for human motion monitoring. *Adv Funct Mater*. 2014;24:4666-4670.
7. Kim KK, Hong S, Cho HM, et al. Highly sensitive and stretchable multidimensional strain sensor with prestrained anisotropic metal nanowire percolation networks. *Nano Lett*. 2015; 15:5240-5247.
8. Ryu S, Lee P, Chou JB, et al. Extremely elastic wearable carbon nanotube fiber strain sensor for monitoring of human motion. *ACS Nano*. 2015;9:5929-5936.
9. Schwartz G, Tee BC-K, Mei J, et al. Flexible polymer transistors with high pressure sensitivity for application in electronic skin and health monitoring. *Nat Commun*. 2013;4:1859.
10. Dagdeviren C, Su Y, Joe P, et al. Conformable amplified lead zirconate titanate sensors with enhanced piezoelectric response for cutaneous pressure monitoring. *Nat Commun*. 2014;5:4496.
11. Bae GY, Pak SW, Kim D, et al. Linearly and highly pressure–sensitive electronic skin based on a bioinspired hierarchical structural Array. *Adv Mater*. 2016;28:5300-5306.
12. You I, Kim B, Park J, et al. Stretchable E-skin apexcardiogram sensor. *Adv Mater*. 2016;28:6359-6364.
13. Smith A. D, Niklaus F, Paussa A, et al. Electromechanical piezoresistive sensing in suspended graphene membranes. *Nano Lett* 2013; 13: 3237–42.
14. Tung TT, Robert C, Castro M, Feller JF, Kim TY, Suh KS. Enhancing the sensitivity of graphene/polyurethane nanocomposite flexible piezo-resistive pressure sensors with magnetite nano-spacers. *Carbon*. 2016;108:450-460.
15. Wu Z-Y, Liang H-W, Hu B-C, Yu S-H. Emerging carbon nanofiber aerogels: chemosynthesis versus biosynthesis. *Angew Chem*. 2018;57(48):15646-15662.
16. Chen C, Song J, Zhu S, et al. Scalable and sustainable approach toward highly compressible, anisotropic, lamellar carbon sponge. *Chem*. 2018;4:544-554.
17. Wegst UG, Bai H, Saiz E, Tomsia AP, Ritchie RO. Bioinspired structural materials. *Nat Mater*. 2015;14:23-36.
18. Chen P-Y, McKittrick J, Meyers MA. Biological materials: functional adaptations and bioinspired designs. *Prog Mater Sci*. 2012;57:1492-1704.
19. Wang K, Lou Z, Wang L, et al. Bioinspired interlocked structure-induced high deformability for two-dimensional titanium carbide (mxene)/natural microcapsule-based flexible pressure sensors. *ACS Nano*. 2019;13(8):9139-9147.
20. Wang L, Wang K, Lou Z, Jiang K, Shen G. Plant–based modular building blocks for "green" electronic skins. *Adv Funct Mater*. 2018;28(51):1804510.
21. Wu Z-Y, Liang H-W, Hu B-C, et al. Emerging carbon nanofiber aerogels: chemosynthesis versus biosynthesis. *Angew Chem*. 2018;57(48):15646-15662.
22. Yang M, Zhao N, Cui Y, et al. Biomimetic architectured graphene aerogel with exceptional strength and resilience. *ACS Nano*. 2017;11:6817-6824.
23. Deville S. Freeze-casting of porous ceramics: a review of current achievements and issues. *Adv Eng Mater*. 2008;10:155-169.
24. Si Y, Wang X, Yan C, Yang L, Yu J, Ding B. Ultralight biomass-derived carbonaceous nanofibrous aerogels with superelasticity and high pressure-sensitivity. *Adv Mater*. 2016;28:9512-9518.
25. Lee J, Kim S, Lee J, et al. A stretchable strain sensor based on a metal nanoparticle thin film for human motion detection. *Nanoscale*. 2014;6:11932-11939.
26. Schaedler TA, Jacobsen AJ, Torrents A, et al. Ultralight metallic microlattices. *Science*. 2011;334:962-965.
27. Liu H, Dong M, Huang W, et al. Lightweight conductive graphene/thermoplastic polyurethane foams with ultrahigh compressibility for piezoresistive sensing. *J Mater Chem C*. 2017;5: 73-83.
28. Sun H, Xu Z, Gao C. Multifunctional, ultra–flyweight, synergistically assembled carbon aerogels. *Adv Mater*. 2013;25:2554-2560.
29. Liu Y, Xu K, Chang Q, et al. Highly flexible and resilient elastin hybrid cryogels with shape memory, injectability, conductivity, and magnetic responsive properties. *Adv Mater*. 2016;28:7758-7767.
30. Wang X, Lu LL, Yu ZL, et al. Scalable template synthesis of resorcinol–formaldehyde/graphene oxide composite aerogels with tunable densities and mechanical properties. *Angew Chem*. 2015;54:2397-2401.
31. Yao B, Chen J, Huang L, Zhou Q, Shi G. Base-induced liquid crystals of graphene oxide for preparing elastic graphene foams with long–range ordered microstructures. *Adv Mater*. 2016;28: 1623-1629.
32. Gao H-L, Zhu Y-B, Mao L-B, et al. Super-elastic and fatigue resistant carbon material with lamellar multi-arch microstructure. *Nat Commun*. 2016;7:12920.
33. Hu H, Zhao Z, Wan W, Gogotsi Y, Qiu J. Ultralight and highly compressible graphene aerogels. *Adv Mater*. 2013;25:2219-2223.
34. Kim P, Abkarian M, Stone HA. Hierarchical folding of elastic membranes under biaxial compressive stress. *Nat Mater*. 2011; 10:952-957.
35. Luo KQ, Vivian CY, Pu Y, Chang DC. Application of the fluorescence resonance energy transfer method for studying the dynamics of caspase-3 activation during UV-induced apoptosis in living HeLa cells. *Biochem Bioph Res Co*. 2001;283:1054-1060.
36. Li YQ, Yu T, Yang TY, Zheng LX, Liao K. Bio-inspired nacre-like composite films based on graphene with superior mechanical, electrical, and biocompatible properties. *Adv Mater*. 2012; 24:3426-3431.

SUPPORTING INFORMATION

Additional supporting information may be found online in the Supporting Information section at the end of this article.

How to cite this article: Chen Y, Hu L, Li C, et al. A biomimetic-structured wood-derived carbon sponge with highly compressible and biocompatible properties for human-motion detection. *InfoMat*. 2020;2:1225–1235. https://doi.org/10.1002/inf2.12075